

A Monte Carlo study of surface critical phenomena: The special point

Martin Hasenbusch*

*Institut für Physik, Humboldt-Universität zu Berlin,
Newtonstr. 15, 12489 Berlin, Germany*

(Dated: February 18, 2022)

Abstract

We study the special point in the phase diagram of a semi-infinite system, where the bulk transition is in the three-dimensional Ising universality class. To this end we perform a finite size scaling study of the improved Blume-Capel model on the simple cubic lattice with two different types of surface interactions. In order to check for the effect of leading bulk corrections we have also simulated the spin-1/2 Ising model on the simple cubic lattice. We have accurately estimated the surface enhancement coupling at the special point of these models. We find $y_{t_1} = 0.718(2)$ and $y_{h_1} = 1.6465(6)$ for the surface renormalization group exponents of the special transition. These results are compared with previous ones obtained by using field theoretic methods and Monte Carlo simulations of the spin-1/2 Ising model. Furthermore we study the behavior of the surface transition near the special point and finally we discuss films with special boundary conditions at one surface and fixed ones at the other.

PACS numbers: 05.50.+q, 05.70.Jk, 05.10.Ln, 68.15.+e

* Martin.Hasenbusch@physik.hu-berlin.de

I. INTRODUCTION

In this paper we shall study the special point in the phase diagram of a semi-infinite system. For reviews on surface critical phenomena see refs. [1–3]. Let us briefly recall the basic features of this phase diagram at the example of the spin-1/2 Ising model on the simple cubic lattice and a semi-infinite geometry. It's reduced Hamiltonian is given by

$$H = -\beta \sum_{\langle xy \rangle} s_x s_y - h \sum_x s_x - \beta_1 \sum_{\langle xy \rangle \in S} s_x s_y - h_1 \sum_{x \in S} s_x, \quad (1)$$

where x and y denote sites of the lattice, $\langle xy \rangle$ is a pair of nearest neighbors and S is the surface of the system. The spin s_x at the site x can take either the value -1 or 1 . The Boltzmann factor is given by $\exp(-H)$, since the reduced Hamiltonian incorporates the temperature. We define $\beta = J/k_B T$, $\beta_1 = J_1/k_B T$, where J is the coupling constant in the bulk, J_1 the excess coupling constant at the surface and T is the temperature. Below we shall refer to β and β_1 as the coupling in the bulk and the excess coupling at the surface, respectively. Below we shall consider vanishing external fields $h = h_1 = 0$ in the bulk as well as at the surface.

In figure 1 we have sketched the phase diagram of this system. For $\beta > \beta_c$, where β_c is the critical coupling of the bulk system, the spins in the bulk are ordered. As a consequence, also the spins at the surface are ordered. At $\beta = 0$ the spins at the surface decouple completely from those of the bulk. Hence a two dimensional Ising model remains that undergoes a phase transition at $\beta_1 = \beta_{c,2D}$. Starting from the point $(0, \beta_{c,2D})$ there is the line of surface transitions, where the spins at the surface order, while those of the bulk remain disordered. This line hits the line (β_c, β_1) in the so called special or surface-bulk point, which is a tricritical point. The transitions from disordered surface and disordered bulk to ordered bulk and ordered surface are called ordinary transitions, while those from disordered bulk and ordered surface to ordered bulk and ordered surface are called extraordinary transitions.

Surface critical phenomena had been studied first by using the mean-field approximation [1]. The application of field theoretic methods to surface critical phenomena is complicated by the fact that translational invariance is broken by the surface. As a consequence, surface critical exponents are only computed up to $O(\epsilon^2)$ in the ϵ -expansion [2, 3]. Furthermore surface critical phenomena have been studied by using high temperature series expansions, real space renormalization group methods and Monte Carlo simulations of lattice models.

The special point is characterized by the two relevant bulk renormalization group (RG)-exponents y_t and y_h and the two relevant surface RG-exponents y_{t_1} and y_{h_1} . Similar to the pure bulk case, these RG-exponents can be related to a number of surface critical exponents that characterize the behavior of thermodynamic quantities related to the surface in the neighborhood of the special point [1–3].

In the present work we locate the special point of three different lattice models and determine the RG-exponents y_{t_1} and y_{h_1} by using finite size scaling (FSS) [4] methods. In the presence of a surface, typically corrections $\propto L^{-1}$ appear [1–3], where L is the linear extent of the finite system. Analysing numerical data, it is difficult to disentangle these corrections from leading bulk corrections which are $\propto L^{-\omega}$, where $\omega = 0.832(6)$ [5]. Therefore, in addition to the Ising model we simulate the Blume-Capel model that is a generalization of the Ising model. In addition to -1 and 1 the spin can take the value 0 . The parameter D of the Blume-Capel model controls the density of spins with $s_x = 0$. It has been shown that for a particular value D^* of the parameter D the amplitude of leading corrections to scaling

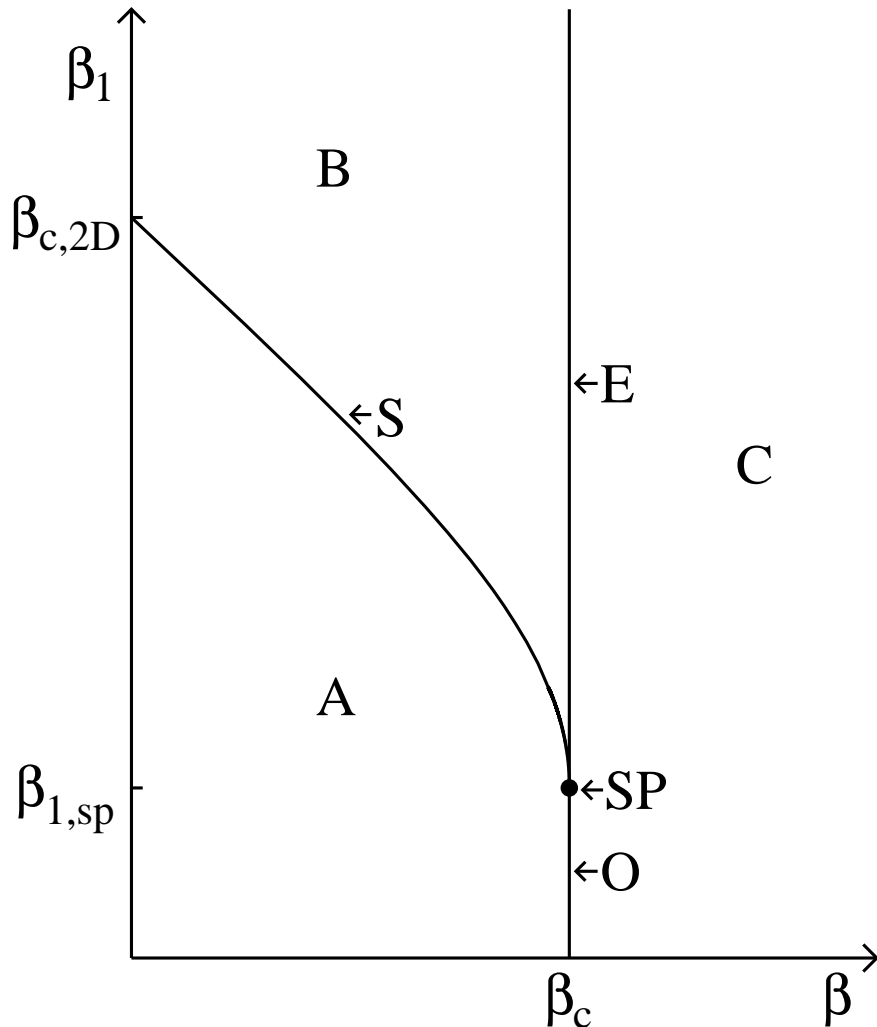


FIG. 1. Sketch of the phase diagram of the semi-infinite system. On the x -axis we plot the coupling β of the bulk and on the y -axis the excess coupling β_1 of the surface. The phase, where both the boundary spins and those of the bulk are disordered is labelled by A, while the one with disordered bulk and ordered surface is labelled by B. The phase, where the bulk and the surface are ordered is labelled by C. The line of surface transitions is labelled by S, the line of ordinary transitions by O and the line of extraordinary transitions by E. These three lines meet in the so called special or surface-bulk point that we have labelled by SP. A discussion is given in the text.

vanishes. See [5] and refs. therein. The precise definition of the model is given below in section II.

The outline of the paper is the following: First we define the models that we simulate. We summarize results for the critical coupling and the critical exponents of the bulk system. We define the quantities that we have measured and discuss their finite size scaling behavior. The scaling behavior is affected by corrections, which have to be taken into account when

analysing Monte Carlo data. Then we report our numerical results: First we have simulated three different models on L^3 lattices, where L is the linear extend of the lattice. Based on these simulations we determine $\beta_{1,sp}$ for these models and obtain estimates of y_{t_1} and y_{h_1} . Next we study the surface transition in the neighborhood of the special point. Then we discuss the magnetisation profile of films with special boundary conditions at one surface and fixed boundary conditions at the other. Finally we summarize and compare our results for the RG-exponents with those obtained by field theoretic methods and previous simulations of the spin-1/2 Ising model.

II. MODELS AND OBSERVABLES

The Blume-Capel model on the simple cubic lattice is characterized by the reduced Hamiltonian

$$H = -\beta \sum_{\langle xy \rangle} s_x s_y + D \sum_x s_x^2 - h \sum_x s_x \quad , \quad (2)$$

where $x = (x_0, x_1, x_2)$ denotes a site of the lattice. The components x_0, x_1 and x_2 take integer values in the range $1 \leq x_i \leq L_i$. The spin s_x might take the values $-1, 0$ or 1 . In the following we shall consider a vanishing external field $h = 0$ throughout. The parameter D controls the density of vacancies $s_x = 0$. In the limit $D \rightarrow -\infty$, these vacancies are completely suppressed, and hence the spin-1/2 Ising model is recovered. For $-\infty \leq D < D_{tri}$ the model undergoes a second order phase transition in the three-dimensional Ising universality class. For $D > D_{tri}$ the transition is of first order. The most recent estimate for the tricritical point is $D_{tri} = 2.0313(4)$ [6]. Numerically, using Monte Carlo simulations it has been shown that there is a point $(D^*, \beta_c(D^*))$ on the line of second order phase transitions, where the amplitude of leading corrections to scaling vanishes. Our most recent estimate is $D^* = 0.656(20)$ [5]. In [5] we have simulated the model at $D = 0.655$ close to β_c on lattices of a linear size up to $L = 360$. From a standard finite size scaling analysis of renormalization group invariant quantities such as the Binder cumulant we found

$$\beta_c(0.655) = 0.387721735(25) \quad (3)$$

for the critical coupling of the bulk at $D = 0.655$. Recent estimates for the critical coupling of the bulk of the spin-1/2 Ising model are $\beta_c = 0.22165455(3)$, table X of [7] and $0.22165463(8)$ [5]. In the following we assume $\beta_c = 0.2216546$. The amplitude of leading corrections to scaling at $D = 0.655$ is at least by a factor of 30 smaller than for the spin-1/2 Ising model.

Our recent estimates for bulk critical exponents in the three-dimensional Ising universality class are [5]

$$\nu = 0.63002(10) \quad , \quad (4)$$

$$\eta = 0.03627(10) \quad , \quad (5)$$

$$\omega = 0.832(6) \quad . \quad (6)$$

A. Film geometry and boundary conditions

In Monte Carlo simulations we are restricted to finite lattices. Therefore a surface requires a counterpart. This means that we actually study systems with a film geometry. In the ideal

case, film geometry means that the system has a finite thickness L_0 , while in the other two directions the thermodynamic limit $L_1, L_2 \rightarrow \infty$ is taken. In order to approximate this limit in Monte Carlo simulations, one usually chooses $L_0 \ll L_1, L_2$ and applies periodic boundary conditions in the 1 and 2 directions. Note that we shall simulate lattices with $L_1 = L_2 = L$ throughout. As we shall see below, in order to compute surface critical exponents, the condition $L_0 \ll L_1, L_2$ is not mandatory. Our estimates for the surface critical exponents are actually obtained from simulations of lattices with $L_0 = L_1 = L_2 = L$.

The reduced Hamiltonian of the Blume-Capel model with film geometry is

$$\begin{aligned}
H = & -\beta \sum_{\langle xy \rangle} s_x s_y + D \sum_x s_x^2 - h \sum_x s_x - \beta_1 \sum_{\langle xy \rangle, x_0=y_0=1} s_x s_y - \beta_2 \sum_{\langle xy \rangle, x_0=y_0=L_0} s_x s_y \\
& + D_1 \sum_{x, x_0=1} s_x^2 + D_2 \sum_{x, x_0=L_0} s_x^2 - h_1 \sum_{x, x_0=1} s_x - h_2 \sum_{x, x_0=L_0} s_x , \tag{7}
\end{aligned}$$

where we have put the surfaces at $x_0 = 1$ and $x_0 = L_0$. In our convention $\langle xy \rangle$ runs over all pairs of nearest neighbor sites with fluctuating spins. Note that here the sites $(1, x_1, x_2)$ and (L_0, x_1, x_2) are not nearest neighbors as it would be the case for periodic boundary conditions. For each bulk term there is a corresponding surface enhancement term. In our simulations and the analysis of the data we have used the surface couplings

$$\bar{\beta}_1 = \beta_1 + \beta \quad \text{and} \quad \bar{\beta}_2 = \beta_2 + \beta \tag{8}$$

as parameters instead of the excess surface couplings β_1 and β_2 .

Note that as long as the bulk transition and the line of surface transitions remain continuous, the qualitative features of the phase diagram that we have discussed in the introduction should remain unchanged. Since the values of D , $D + D_1$ and $D + D_2$ that we shall consider are much smaller than $D_{tri} = 2.0313(4)$ [6] and $D_{tri,2D} = 1.966(2)$ [8] of the two-dimensional Blume-Capel model on the square lattice, this should be the case in our study.

B. Observables

Renormalization group invariant quantities are very useful to locate critical or multicritical points. We study the Binder cumulant

$$U_4 = \frac{\langle m^4 \rangle}{\langle m^2 \rangle^2} , \tag{9}$$

where $m = \sum_x s_x$. The second moment correlation length is given by

$$\xi_{2nd} = \sqrt{\frac{\chi/F - 1}{4 \sin^2 \pi/L}} , \tag{10}$$

where

$$F = \frac{1}{L_0 L^2} \left\langle \left| \sum_x \exp \left(i \frac{2\pi x_{1,2}}{L_{1,2}} \right) s_x \right|^2 \right\rangle \tag{11}$$

is the Fourier transform of the correlation function at the lowest non-zero momentum in 1 or 2 direction and $\chi = \langle m^2 \rangle / (L_0 L^2)$ is the magnetic susceptibility. Since in our simulations

$L_1 = L_2$, the expectation value of F is identical for the 1 and the 2 direction. In order to reduce the statistical error, we have measured F for both directions and have averaged the results. The ratio ξ_{2nd}/L is renormalization group invariant. The third renormalization group invariant quantity that we consider is the ratio Z_a/Z_p of partition functions, where Z_a is the partition function of a system with anti-periodic boundary conditions in 1 direction and periodic ones in 2 direction or vice versa, while in the case of Z_p periodic boundary conditions are imposed in 1 and 2 direction. Also here, since $L_1 = L_2$ in our simulations, we determine Z_a/Z_p for both choices and average the results. The ratio Z_a/Z_p of partition functions can be efficiently evaluated using the boundary flip algorithm [9]. Here we use a modified version of the boundary flip algorithm as discussed in appendix A 2 of ref. [10]. In the following we shall refer to the renormalization group invariant quantities U_4 , Z_a/Z_p and ξ_{2nd}/L using the symbol R . For vanishing symmetry breaking fields $h = h_1 = h_2 = 0$, $D_1 = D_2$ and $\beta_1 = \beta_2$, a renormalization group invariant quantity behaves as

$$R(L_0, L, \beta, \beta_1) = q(L/L_0, t[L_0/\xi_0]^{y_t}, t_1[L_0/\xi_{1,0}]^{y_{t_1}}) , \quad (12)$$

where $t = \beta_c - \beta$, $t_1 = \beta_{1,sp} - \beta_1$, ξ_0 is the amplitude of the correlation length in the high temperature phase and the normalisation factor $\xi_{1,0}$ is still undetermined. In section (III) we have fixed the ratio $L/L_0 = 1$ and have set the bulk coupling to its critical value: $\beta = \beta_c$. This allows us to determine the location of the special point $\beta_{1,sp}$ by using the standard crossing method, where R is considered as function of β_1 . The behavior of the slope of the renormalization group invariant quantities allows us to determine the surface RG-exponent y_{t_1} : Taking the derivative with respect to β_1 we get

$$\frac{\partial R(L_0, L, \beta, \beta_1)}{\partial \beta_1} = Q(L/L_0, t[L_0/\xi_0]^{y_t}, t_1[L_0/\xi_{1,0}]^{y_{t_1}}) [L_0/\xi_{1,0}]^{y_{t_1}} \quad (13)$$

where Q is minus the partial derivative of q with respect to its third argument.

Finally we define the surface susceptibilities for a vanishing surface magnetisation $\langle m_1 \rangle$:

$$\chi_{11} = \frac{\partial \langle m_1 \rangle}{\partial h_1} = L^2 \langle m_1^2 \rangle \quad (14)$$

where

$$m_1 = \frac{1}{L^2} \sum_{x_1, x_2} s^{(1, x_1, x_2)} \quad (15)$$

and

$$\chi_{12} = \frac{\partial \langle m_1 \rangle}{\partial h_2} = L^2 \langle m_1 m_2 \rangle \quad (16)$$

where

$$m_2 = \frac{1}{L^2} \sum_{x_1, x_2} s^{(L_0, x_1, x_2)} . \quad (17)$$

The finite size scaling behavior of these quantities can be inferred from the singular part of the reduced free energy per area of the film. Its scaling form is

$$f_s(\dots, \dots, \dots, h_1, h_2) = L_0^{-d+1} g(L/L_0, \dots, \dots, h_1[L_0/l_{h_1}]^{y_{h_1}}, h_2[L_0/l_{h_2}]^{y_{h_2}}) , \quad (18)$$

where the constants l_{h_1} and l_{h_2} remain undetermined here. y_{h_1} and y_{h_2} are the RG-exponents related to the surface fields. The susceptibilities defined above can be expressed as second

derivatives of f_s with respect to the surface fields. Taking these derivatives on the right hand side of eq. (18) we arrive at

$$\chi_{11} = \frac{\partial^2 f_s}{\partial h_1^2} = cL_0^{-d+1}[L_0/l_{h_1}]^{2y_{h_1}} \quad (19)$$

and

$$\chi_{12} = \frac{\partial^2 f_s}{\partial h_1 \partial h_2} = cL_0^{-d+1}[L_0/l_{h_1}]^{y_{h_1}}[L_0/l_{h_2}]^{y_{h_2}} \quad (20)$$

In our study below, section III B, $y_{h_1} = y_{h_2}$ and $l_{h_1} = l_{h_2}$, since we have chosen $\beta_1 = \beta_2$, $D_1 = D_2$ and $h_1 = h_2 = 0$.

C. Corrections to scaling

Finite size scaling laws such as eqs. (12,13,19,20) are affected by corrections. These are caused by irrelevant scaling fields, the analytic background in the reduced free energy per area and the fact that e.g. in eq. (12) the arguments of the scaling function q should be actually analytic functions of t and t_1 that we have linearized here.

The leading bulk correction is $\propto L_0^{-\omega}$, where our most recent estimate $\omega = 0.832(6)$ obtained from Monte Carlo simulations of the Blume-Capel and the Ising model [5] is slightly larger than that obtained from field theoretical methods, e.g. $\omega = 0.799(11)$ by using perturbation theory in three dimensions fixed and $\omega = 0.814(14)$ by using the ϵ -expansion [11]. There are also corrections $\propto L_0^{-n\omega}$, where $n = 2, 3, \dots$. In the case of improved models these are highly suppressed and therefore we shall ignore them in the analysis of our data below. Following [12] subleading corrections are characterized by $\omega_2 = 1.67(11)$. There is no reason to assume that the amplitude of the subleading correction vanishes in the case of the improved Blume-Capel model. Likely it is of similar size as in the spin-1/2 Ising model. Furthermore there are well established corrections with $\omega_i \approx 2$, for example related to the breaking of the spatial rotational invariance by the simple cubic lattice [13].

In the presence of surfaces there are also corrections caused by irrelevant surface fields. One expects that the leading ones are $\propto L_0^{-1}$ [1-3].

In general we expect that for finite L_0 finite size scaling laws such as eqs. (13,19,20) can be written in the form of a Wegner-expansion [14]

$$A(L_0) = cL_0^x[1 + aL_0^{-\omega} + \sum_{i=2} a_i L_0^{-\omega_i}] \quad (21)$$

with an infinite number of correction terms. Fitting data obtained from Monte Carlo simulations, only a very limited number of terms can be taken into account. This unavoidable truncation of the Wegner-expansion leads to a systematic error of the estimate of e.g. the exponent x that is often larger than the statistical one.

In the present work, we shall use ansaetze that include either no correction, a correction $\propto L_0^{-1}$ or corrections $\propto L_0^{-1}$ and $\propto L_0^{-2}$. In the case of the surface susceptibilities we shall also take into account a term for the analytic background. The systematic errors of our results are then estimated from the variation of the results obtained by using these different ansaetze.

TABLE I. Number of measurements divided by 10^6 . For each measurement we perform one heat-bath sweep, a certain number of single cluster and two wall-cluster updates.

L	BC1	BC2	Ising
8	1000	1000	1000
12	1000	1000	1000
16	1000	1000	1000
24	1000	1178	877
32	1020	1042	718
48	861	705	305
64	593	482	224
96	301	200	132
128	202	140	116

III. SIMULATIONS OF L^3 LATTICES AT THE SPECIAL POINT

In this part of our study we consider three different models. In all cases we chose $L_0 = L$, $\bar{\beta}_1 = \bar{\beta}_2$, $D_1 = D_2$ and $h_1 = h_2 = 0$. We have simulated the Blume-Capel model at $D = 0.655$ with two different choices of D_1 : The choice $D_1 = 0$ is called BC1 model and $D_1 \rightarrow -\infty$ is called BC2 model in the following. Note that in the case of the BC2 model, the spins at the surfaces can take only the values -1 or 1 . In addition, we have simulated the spin-1/2 Ising model. We have simulated at the best estimates of the bulk critical point; i.e. $\beta_c = 0.387721735$ for the Blume Capel model at $D = 0.655$ and $\beta_c = 0.2216546$ for the spin-1/2 Ising model. The numerical uncertainty of these numbers is negligible in the present study.

For each measurement of the observables we performed the following sequence of Monte Carlo updates: First one sweep with a local update. In the case of the Ising model we use a local Metropolis and for the Blume-Capel model a local heat-bath update. One sweep means that we run through the lattice once in type-writer fashion. Then we performed a certain number of single-cluster updates [15] followed by two wall-cluster updates [16]; one for each of the directions with periodic boundary conditions. In all our simulations we have used the Mersenne twister algorithm [17] as pseudo-random number generator.

In the case of the Blume-Capel models BC1 and BC2, no previous estimate of the surface coupling $\bar{\beta}_{1,sp}$ was available. Therefore, we have successively improved our estimate of $\bar{\beta}_{1,sp}$ with increasing lattice size L . In order to obtain the observables as a function of $\bar{\beta}_1$ in the neighborhood of the simulation point, we have computed the coefficients of the Taylor-expansion of the observables in $\bar{\beta}_1$ around the simulation point up to third order. In table I we summarize the lattice sizes that we have simulated at and the statistics of these simulations. In total we have spent about 12 years of CPU time on a single core of a Quad-Core AMD Opteron(tm) Processor 2378 running at 2.4 GHz.

In our simulations we have measured the renormalization group invariant quantities Z_a/Z_p , U_4 and ξ_{2nd}/L . Analysing the data, it turned out that corrections to scaling are considerably larger for ξ_{2nd}/L than for Z_a/Z_p and U_4 . Therefore we restrict the following discussion to Z_a/Z_p and U_4 .

TABLE II. Fitting the ratio of partition functions Z_a/Z_p for the BC1 model with the ansaetze (22), (24) or (25).

Ansatz	L_{min}	$\bar{\beta}_{1,sp,BC1}$	$(Z_a/Z_p)^*$	c	d	χ^2/DOF
22	32	0.5491558(23)	0.31318(5)			14.2/3
22	48	0.5491482(32)	0.31341(8)			2.32/2
24	16	0.5491430(33)	0.31374(10)	0.0131(14)		6.08/4
24	24	0.5491350(47)	0.31406(17)	0.0194(31)		0.69/3
25	12	0.5491423(49)	0.31375(19)	0.0121(47)	0.023(34)	8.87/4
25	16	0.5491280(69)	0.31445(32)	0.035(10)	-0.216(94)	0.51/3

In a first step of the analysis we have computed the surface coupling $\bar{\beta}_{1,sp}$ of the special point and the fixed point values of Z_a/Z_p and U_4 . To this end we have fitted the data with the ansatz

$$R(\bar{\beta}_{1,sp}, L) = R^* \quad (22)$$

where $\bar{\beta}_{1,sp}$ and R^* are the free parameters of the fit and

$$R(\bar{\beta}_{1,sp}, L) = R(\bar{\beta}_{1,s}, L) + c_1(\bar{\beta}_{1,sp} - \bar{\beta}_{1,s}) + \frac{c_2}{2!}(\bar{\beta}_{1,sp} - \bar{\beta}_{1,s})^2 + \frac{c_3}{3!}(\bar{\beta}_{1,sp} - \bar{\beta}_{1,s})^3 \quad (23)$$

where $R(\bar{\beta}_{1,s}, L)$, c_1 , c_2 and c_3 are obtained from the simulation at $\bar{\beta}_{1,s}$. To check for the possible effect of corrections to scaling we have also used the ansaetze

$$R(\bar{\beta}_{1,sp}, L) = R^* + cL^{-1} \quad (24)$$

and

$$R(\bar{\beta}_{1,sp}, L) = R^* + cL^{-1} + dL^{-2} \quad (25)$$

First we have analyzed the three models separately. Let us first look at the results for the BC1 model and the ratio Z_a/Z_p . A selection of results is given in table II. In these fits we have taken into account the data for all lattice sizes $L \geq L_{min}$. Fits with an acceptable χ^2/DOF are obtained starting from $L_{min} = 48, 24$ and 16 for the ansaetze (22), (24) and (25), respectively. Note that the differences of the results for $\bar{\beta}_{1,sp}$ and $(Z_a/Z_p)^*$ for different ansaetze with an acceptable χ^2/DOF are larger than the statistical errors. Next we have fitted the Binder cumulant with the ansaetze (22), (24) and (25). In the case of the ansatz (22) we find $\chi^2/\text{DOF} = 1.32/4$ already for $L_{min} = 24$ with $\bar{\beta}_{1,sp} = 0.5491393(32)$ and $U_4^* = 1.52338(7)$. Fitting the data for $L_{min} = 8$ with the ansaetze (24) and (25) we get $\chi^2/\text{DOF} = 8.69/6$ and $8.61/5$, respectively. The results for the fit parameters are $\bar{\beta}_{1,sp} = 0.5491470(37)$, $U_4 = 1.52303(10)$ and $\bar{\beta}_{1,sp} = 0.5491455(63)$, $U_4 = 1.52309(23)$, for the ansaetze (24) and (25), respectively. Notice that the results for $\bar{\beta}_{1,sp}$ are compatible with those obtained from the analysis of Z_a/Z_p .

Next we have analyzed the data for the BC2 model. In the case of the ansatz (22) larger L_{min} are needed than for the BC1 model to get an acceptable χ^2/DOF . Fitting the data with the ansaetze (24) and (25) we see that the correction amplitude c is clearly larger for the BC2 than for the BC1 model.

Next we performed joint fits for the BC1 and the BC2 model using the ansaetze (24) and (25). In these fits we impose that, following universality, $(Z_a/Z_p)^*$ and U_4^* are the same for

TABLE III. Fitting the ratio of partition functions Z_a/Z_p for the BC1 and BC2 model with the ansätze (24) or (25). In the case of ansatz (25) we do not report d_1 and d_2 to keep the table readable.

Ansatz	L	$\bar{\beta}_{1,sp,BC1}$	$\bar{\beta}_{1,sp,BC2}$	$(Z_a/Z_p)^*$	c_1	c_2	χ^2/DOF
24	12	0.5491418(20)	0.2940123(19)	0.31380(5)	0.0144(6)	-0.0782(6)	19.78/11
24	16	0.5491461(24)	0.2940165(23)	0.31364(7)	0.0118(10)	-0.0806(10)	9.36/9
24	24	0.5491416(35)	0.2940124(33)	0.31382(13)	0.0152(23)	-0.0771(22)	6.20/7
25	8	0.5491493(27)	0.2940202(26)	0.31346(9)	0.0045(17)	-0.0863(16)	15.44/11
25	12	0.5491481(28)	0.2940189(36)	0.31352(15)	0.0064(38)	-0.0850(37)	15.13/9
25	16	0.5491364(52)	0.2940086(49)	0.31407(23)	0.0242(70)	-0.0664(68)	4.70/7

TABLE IV. Same as table III but for the Binder cumulant U_4 instead of Z_a/Z_p .

Ansatz	L	$\bar{\beta}_{1,sp,BC1}$	$\bar{\beta}_{1,sp,BC2}$	U_4^*	c_1	c_2	χ^2/DOF
24	16	0.5491396(42)	0.2940168(40)	1.52327(13)	-0.005(2)	0.347(2)	16.75/9
24	24	0.5491377(61)	0.2940104(57)	1.52345(23)	0.002(4)	0.348(4)	1.95/7
25	8	0.5491520(45)	0.2940194(41)	1.52285(15)	-0.011(3)	0.323(3)	13.58/11
25	12	0.5491517(66)	0.2940202(62)	1.52284(27)	-0.012(7)	0.324(7)	13.00/9
25	16	0.5491342(82)	0.2940047(80)	1.52372(38)	0.017(12)	0.353(11)	5.84/7

both models. A selection of results is given in table III. We see that the correction amplitude c_2 of the BC2 model is much larger than c_1 of the BC1 model. We performed similar fits for the Binder cumulant U_4 . Also here we observe that the correction $\propto L^{-1}$ has a much larger amplitude for the BC2 model than for the BC1 model. The results for the surface couplings at the special point $\bar{\beta}_{1,sp,BC1}$ and $\bar{\beta}_{1,sp,BC2}$ obtained from the analysis of U_4 and Z_a/Z_p are compatible among each other.

As our final result we quote

$$(Z_a/Z_p)^* = 0.3138(5) \quad , \quad U_4^* = 1.5234(10) \quad (26)$$

and

$$\bar{\beta}_{1,sp,BC1} = 0.54914(2) \quad , \quad \bar{\beta}_{1,sp,BC2} = 0.29401(2) \quad (27)$$

where the error bars are chosen such that the results of all fits given in table III and IV are covered.

Finally we have fitted our data for the spin-1/2 Ising model using the ansatz (24). A selection of results is given in table V. For $L_{min} = 16$ and 24 we find acceptable values for χ^2/DOF . Nevertheless the result for $(Z_a/Z_p)^*$ is not compatible with that obtained from the fits for the BC1 and BC2 models. This could be explained by the fact that corrections $\propto L^{-\omega}$ with $\omega = 0.832(6)$ [5] are not explicitly taken into account.

Finally we performed a number of different fits, where we take the results (26) for $(Z_a/Z_p)^*$ and U_4^* as input. In these fits we also include explicitly corrections $\propto L^{-\omega}$. Taking into

TABLE V. Fitting the ratio of partition functions Z_a/Z_p for the spin-1/2 Ising model with the ansatz (24).

L	$\bar{\beta}_{1,sp,I}$	$(Z_a/Z_p)^*$	c	χ^2/DOF
12	0.3330388(15)	0.31221(5)	0.00219(5)	9.03/5
16	0.3330365(19)	0.31232(7)	0.00236(9)	4.34/4
24	0.3330338(28)	0.31246(13)	0.00262(23)	2.77/3

TABLE VI. Comparison of our result for the ratio $\bar{\beta}_{1,sp,I}/\beta_c$ with those given in the literature.

Ref.	year	$\bar{\beta}_{1,sp,I}/\beta_c$
[18]	1984	1.50(3)
[19]	1990	1.52(2)
[20]	1993	1.5004(20)
[21]	2005	1.50208(5)
Here	2011	1.50243(9)

account these different fits we arrive at the final estimate

$$\bar{\beta}_{1,sp,I} = 0.33302(2) \quad (28)$$

for the spin-1/2 Ising model. In table VI we compare our result with those given in the literature. Our result is compatible within error bars with all others except for the one of ref. [21], where we find that the difference is 2.5 times larger than the combined error.

A. The RG-exponent y_{t_1}

We have determined the critical exponent y_{t_1} from the slope of a renormalization group invariant quantity R_1 at a fixed value $R_{2,f}$ of a second renormalization group invariant quantity R_2

$$\bar{S} := \left. \frac{\partial R_1}{\partial \beta_1} \right|_{R_2=R_{2,f}} \simeq cL^{y_{t_1}} \quad , \quad (29)$$

where in our case R_1 is either the Binder cumulant U_4 or the ratio of partition functions Z_a/Z_p and we fix $(Z_a/Z_p)_f = 0.3138$. Fitting our data we have used the ansatz

$$\bar{S} = cL^{y_{t_1}} \quad , \quad (30)$$

$$\bar{S} = cL^{y_{t_1}}(1 + dL^{-1}) \quad , \quad (31)$$

and

$$\bar{S} = cL^{y_{t_1}}(1 + dL^{-1} + eL^{-2}) \quad . \quad (32)$$

In table VII the results of fits for the slope of Z_a/Z_p at $Z_a/Z_p = 0.3138$ for the BC1 model are given. We also performed joint fits of the BC1 and the BC2 model. In table VIII we

TABLE VII. *Fitting the slope of Z_a/Z_p at $Z_a/Z_p = 0.3138$ for the BC1 model.*

Ansatz	L_{min}	y_{t_1}	d	e	χ^2/DOF
30	32	0.71909(21)			4.26/3
30	48	0.71855(36)			0.89/2
31	12	0.71583(28)	-0.148(6)		20.91/5
31	16	0.71700(38)	-0.108(11)		1.57/4
32	8	0.71795(49)	-0.026(21)	-0.71(9)	5.39/5
32	12	0.71872(82)	0.022(49)	-1.01(30)	3.75/4

TABLE VIII. *Fitting the slope of Z_a/Z_p at $Z_a/Z_p = 0.3138$ for the BC1 and the BC2 model jointly.*

Ansatz	L_{min}	y_{t_1}	d_1	d_2	e_1	e_2	χ^2/DOF
31	16	0.71694(29)	-0.109(9)	0.354(9)			7.18/9
31	24	0.71758(50)	-0.084(21)	0.386(21)			3.76/7
32	8	0.71792(29)	-0.027(11)	0.436(13)	-0.71(4)	-0.69(5)	10.87/11
32	12	0.71898(60)	0.037(32)	0.505(32)	-1.09(19)	-1.12(19)	4.86/9

report results obtained from the slope of Z_a/Z_p at $Z_a/Z_p = 0.3138$. Also in the case of the slopes we observe that the amplitude of L^{-1} corrections is much larger for the BC2 than for the BC1 model. Therefore using ansatz (30) no acceptable fit can be obtained.

Based on these fits we arrive at the final estimate

$$y_{t_1} = 0.718(2) . \quad (33)$$

The central value and the error bar are chosen such that all the results of the fits reported in tables VII and VIII are covered. Our final estimate is also consistent with the results obtained from the slope of the Binder cumulant U_4 . We have also fitted our data for the Ising model with the ansaetze (30,31,32). The results obtained from the slope of Z_a/Z_p for y_{t_1} are fully consistent with the estimate (33), while those from the slope of U_4 are a bit larger. We conclude that leading bulk corrections $\propto L^{-\omega}$ have only a small numerical effect in the case of the Ising model and can therefore be savely ignored in the case of the Blume-Capel model at $D = 0.655$, where leading corrections to scaling are suppressed at least by a factor of 30 compared with the Ising model.

B. Surface susceptibilities and the RG-exponent y_{h_1}

Finally we have determined the exponent y_{h_1} from the finite size scaling behavior of the surface susceptibilities χ_{11} and χ_{12} . To this end we have computed

$$\bar{\chi} := \chi|_{R=R_f} \propto L^{2y_{h_1} - 2} \quad (34)$$

where we use $(Z_a/Z_p)_f = 0.3138$. We have fitted these quantities with the ansaetze

$$\bar{\chi} = cL^x \quad (35)$$

TABLE IX. Fitting the surface susceptibilities χ_{11} and χ_{12} at $Z_a/Z_p = 0.3138$. Both the data of the BC1 and the BC2 model are taken into account. Results for the parameters b and e are not reported to keep the table readable.

Quantity	Ansatz	L_{min}	x	d_1	d_2	χ^2/DOF
$\bar{\chi}_{11}$	36	24	1.2930(3)	-0.09(1)	1.13(1)	10.37/7
$\bar{\chi}_{11}$	36	32	1.2932(4)	-0.09(2)	1.15(2)	4.48/5
$\bar{\chi}_{11}$	37	16	1.2935(4)	-0.08(5)	1.39(6)	6.87/7
$\bar{\chi}_{11}$	38	8	1.2933(6)	-0.19(15)	1.12(15)	8.56/9
$\bar{\chi}_{12}$	36	24	1.2921(2)	-0.36(1)	0.02(1)	4.01/7
$\bar{\chi}_{12}$	36	32	1.2922(3)	-0.35(1)	0.03(1)	2.96/5
$\bar{\chi}_{12}$	37	16	1.2932(4)	-0.19(6)	0.35(6)	10.28/7
$\bar{\chi}_{12}$	37	24	1.2927(5)	-0.25(12)	0.16(13)	3.10/5
$\bar{\chi}_{12}$	38	8	1.2935(2)	-0.13(2)	0.32(5)	14.61/9
$\bar{\chi}_{12}$	38	12	1.2929(3)	-0.30(4)	0.02(9)	7.83/7
$\bar{\chi}_{12}$	38	16	1.2928(6)	-0.14(17)	-0.06(25)	3.19/5

where $x = 2y_{h_1} - 2$,

$$\bar{\chi} = cL^x(1 + dL^{-1}) , \quad (36)$$

$$\bar{\chi} = cL^x(1 + dL^{-1}) + b \quad (37)$$

where b is an analytic background and

$$\bar{\chi} = cL^x(1 + dL^{-1} + eL^{-2}) + b . \quad (38)$$

It turns out that using the ansatz (35) for none of the models studied an acceptable fit can be obtained. In table IX results of joint fits of the BC1 and the BC2 model using the ansatz (36,37,38) are reported. The variation of the results for the parameter x with the different ansatz is of similar size as the statistical errors. The results obtained from χ_{11} are slightly larger than those from χ_{12} . Our final estimate $x = 1.2929(10)$ covers all results reported in table IX. Fitting the data obtained for the Ising model we get results for the parameter x that are essentially consistent with that obtained for the Blume-Capel models BC1 and BC2. Therefore residual leading bulk corrections in the case of the Blume-Capel model at $D = 0.655$ should not affect our final estimate of x . As our final estimate for the RG-exponent of the external surface field we quote

$$y_{h_1} = 1.6465(6) . \quad (39)$$

IV. NUMERICAL RESULTS FOR THE SURFACE TRANSITION

In the neighborhood of the special point, the transition line behaves as [1-3]

$$|t_{1,c}| = c|t|^\Phi , \quad (40)$$

where $\Phi = \nu y_{t_1}$ is the cross-over exponent. In the present section we shall compute the line of surface transitions numerically and check how well it is described by eq. (40). To this

TABLE X. Value of $\bar{\beta}_{1,c}$ obtained by requiring that $Z_a/Z_p = 0.372884880824589\dots$ as a function of L_0 and L . Throughout $\beta = 0.31$.

L_0	L	$\bar{\beta}_{1,c}$
10	8	0.6738189(96)
10	10	0.6739017(78)
10	12	0.6739022(65)
10	20	0.6738941(40)
10	100	0.6738924(95)
5	100	0.6739308(83)
6	100	0.6739055(86)
7	100	0.6738980(85)
8	100	0.6738761(85)
12	100	0.6738845(82)

end, we have only simulated the BC1 model, i.e. the Blume-Capel model at $D = 0.655$ and $D_1 = D_2 = 0$, since it has the smallest scaling corrections among the three models discussed in the preceding section. For given values of the bulk coupling $\beta < \beta_c$ we have determined the critical surface coupling $\bar{\beta}_{1,c}$. To this end we have simulated films with an excess surface coupling $\beta_1 > 0$ at one surface and free boundary conditions, i.e. $\beta_2 = 0$, at the other. For $L_0 \gg \xi$, where ξ is the correlation length of the bulk, the film should provide a good approximation of the semi-infinite system. We have determined $\bar{\beta}_{1,c}$ by requiring that the ratio of partition functions Z_a/Z_p assumes the fixed point value of a square system with periodic boundary conditions in the universality class of the two-dimensional Ising model [22]

$$(Z_a/Z_p)^* = 0.372884880824589\dots \quad (41)$$

In the case of Z_a/Z_p corrections to the fixed point value of the two-dimensional Ising universality class vanish $\propto L^{-4}$ [23]. Note that in the case of U_4 and ξ_{2nd}/L the analytic background of the magnetisation enters. Therefore, for these two quantities corrections vanish $\propto L^{-7/4}$.

Similar to the previous section, we have updated the configurations by using a hybrid of the local heat-bath algorithm, the single-cluster algorithm and the wall-cluster algorithm. First we performed a series of simulations with varying values of L_0 and L at $\beta = 0.31$, where $\xi_{2nd} = 1.04430(21)$. Our results are summarized in table X. We expect that corrections to the limit $L_0, L \rightarrow \infty$ decay exponentially with increasing L_0 and power-like as L increases. We see that for $L = 20$ and $L_0 = 10$ the corrections are smaller than the statistical error of our numerical results. Assuming scaling, we chose for our simulations at larger values of β the lattice size such that $L_0 > 10\xi$ and $L = 2L_0$. The numerical results of these simulations are summarized in table XI. In total these simulations took about 8 month of CPU time on a single core of a Quad-Core AMD Opteron(tm) Processor 2378 running at 2.4 GHz.

In order to check the prediction (40) we have fitted our data with the ansatz

$$\bar{\beta}_{1,c} = \bar{\beta}_{1,sp} + a \left(t + \sum_{i=2}^m c_i t^i \right)^\Phi \quad (42)$$

TABLE XI. The surface coupling $\bar{\beta}_{1,c}$ at the surface transition for various values of the bulk coupling β . In addition we give the second moment correlation length ξ_{2nd} of the bulk system, the linear lattice sizes L_0 and L and the number of measurements (stat).

β	ξ_{2nd}	L_0	L	stat/ 10^5	$\bar{\beta}_{1,c}$
0.36	2.1272(4)	24	48	100	0.6394276(58)
0.378	4.1937(7)	50	100	100	0.6093666(31)
0.3822	6.0133(7)	70	140	100	0.5967239(25)
0.3842	7.9984(13)	100	200	35	0.5883957(31)
0.3859	12.1358(22)	150	300	20.2	0.5785822(31)
0.3865	15.6127(28)	180	360	22.5	0.5738132(27)
0.3869	20.0576(45)	250	500	6.9	0.5698232(38)

TABLE XII. Fitting the critical surface coupling $\bar{\beta}_{1,c}$ with the ansatz (42), where $m - 1$ gives the number of correction terms that are included. For a discussion see the text.

m	$\bar{\beta}_{1,min}$	$\bar{\beta}_{1,sp}$	a	c_2	c_3	χ^2/DOF
3	0.36	0.549350(9)	0.51156(18)	-11.27(7)	114.7(1.9)	51.6/3
3	0.378	0.549222(20)	0.51490(50)	-13.60(33)	266(21)	0.77/2
2	0.378	0.549454(7)	0.50893(14)	-9.45(4)		154/3
2	0.3822	0.549310(14)	0.51236(32)	-10.99(13)		10.1/2
2	0.3842	0.549240(26)	0.51419(66)	-12.15(39)		0.00/1
1	0.3842	0.549993(7)	0.49483(12)			877/2
1	0.3859	0.549642(14)	0.50214(28)			28.8/1
1	0.3865	0.549519(27)	0.50492(59)			-

where we have fixed $\Phi = \nu y_{t_1} = 0.63002 \times 0.718$. Our results are summarized in table XII. We see that without any correction, even the fit that includes only the three largest values of β that we have simulated has a very large χ^2/DOF and the result for $\bar{\beta}_{1,sp}$ is by far too large compared with that obtained in the previous section. Adding corrections terms, smaller values of β can be included into the fits. Also the value of $\bar{\beta}_{1,sp}$ gets closer to our result obtained above when adding further correction terms. However, the values of the correction amplitudes are large and rapidly increase with increasing order. We conclude that the behavior of the surface transition seems to be consistent with the theoretical expectation (40). However an accurate estimate of $\bar{\beta}_{1,sp}$ cannot be obtained from the numerical analysis of the surface transition. Finally we have performed a fit, where we have fixed $\bar{\beta}_{1,sp}$ as well as the crossover exponent Φ . Including all data with $\beta \geq 0.378$ we get

$$\bar{\beta}_{1,c}(\beta) = 0.54914 + 0.51736(12)[t - 16.7(4)t^2 + 752(101)t^3 - 25015(6205)t^4]^{0.63002 \times 0.718} \quad (43)$$

where $t = 0.387721735 - \beta$ with $\chi^2/\text{DOF} = 1.23/2$. This result might be helpful in future studies of the surface transition in the BC1 model.

V. FILMS WITH (SP,+) BOUNDARY CONDITIONS

Finally we have simulated the BC1 model with special boundary conditions at one surface and + boundary conditions at the other, where + boundary conditions means that there are spins at $x_0 = L_0 + 1$ which are fixed to +1, which is equivalent to $h_2 = \beta$. We have simulated at $\beta = \beta_c$ and $\bar{\beta}_1 = \bar{\beta}_{1,s} = 0.549145$, which was our preliminary estimate of $\bar{\beta}_{1,sp}$ at the time, when we started the simulations. We have measured the magnetisation profile. We have computed the Taylor expansion of the magnetisation profile in $\bar{\beta}_1$ around the simulation point $\bar{\beta}_{1,s}$ up to the second order. For each measurement we performed the following sequence of Monte Carlo updates: One sweep with the local heat-bath update, a cluster-update, one sweep with the local heat-bath update, and again a cluster-update. In these cluster-updates we flip the sign of the frozen boundary and all spins of the cluster attached to it. Performing this cluster update twice, we are back to + boundary conditions at the surface.

Mainly, we have simulated lattices with $L = 4 \times L_0$. We have checked that at the level of our accuracy, deviations from the effectively two-dimensional thermodynamic limit $L/L_0 \rightarrow \infty$ are negligible for this choice. To this end we have simulated $L = 24, 32$ and 48 for the thickness $L_0 = 8$. The results obtained for $L = 32$ and 48 are consistent among each other and those for $L = 24$ deviate only little. For $L = 4 \times L_0$, we have studied films of the thicknesses $L_0 = 6, 8, 12, 16, 24, 32, 48, 64, 96$ and 128 . We have performed $10^9, 5 \times 10^8, 10^8, 10^8, 10^8, 6 \times 10^7, 4 \times 10^7, 2.6 \times 10^7, 1.5 \times 10^7$ and 7.7×10^6 measurements for these lattice sizes, respectively. In total these simulations took a bit more than 2 years of CPU-time on a single core of a Quad-Core AMD Opteron(tm) Processor 2378 running at 2.4 GHz.

A. The magnetization at the boundary

First let us discuss the behavior of the magnetisation m_1 at the boundary as a function of the thickness of the film. In terms of the reduced free energy per area it is given by

$$\begin{aligned} \frac{\partial f(L_0, t, h, t_1, h_1)}{\partial h_1} &= \frac{1}{L^2} \frac{1}{Z} \frac{\sum_{\{s\}} \exp(\dots + h_1 \sum_{x_1, x_2} s_{(1, x_1, x_2)})}{\partial h_1} \\ &= \frac{1}{L^2} \left\langle \sum_{x_1, x_2} s_{(1, x_1, x_2)} \right\rangle = m_1 \quad . \end{aligned} \quad (44)$$

Note that the non-singular contribution to the free energy from the first surface does not feel the breaking of the symmetry by the second surface. Therefore it is an even function of h_1 and does not contribute to the partial derivative with respect to h_1 . Similar to eq. (18) the singular part of the reduced free energy per area behaves as

$$f_s(L_0, t, h, t_1, h_1) = L_0^{-d+1} g(\dots, h_1 [L_0/l_{h_1}]^{y_{h_1}}) \quad . \quad (45)$$

Taking the partial derivative with respect to h_1 we get

$$\begin{aligned} m_1 &= \left. \frac{\partial f_s}{\partial h_1} \right|_{t=h=t_1=h_1=0} = L_0^{-d+1} \left. \frac{\partial g(\dots, h_1 [L_0/l_{h_1}]^{y_{h_1}})}{\partial h_1} \right|_{t=h=t_1=h_1=0} \\ &= L_0^{-d+1} g_{h_1}(0, 0, 0, 0) \Big|_{t=h=t_1=h_1=0} [L_0/l_{h_1}]^{y_{h_1}} = c L_0^{-d+1+y_{h_1}} \quad , \end{aligned} \quad (46)$$

TABLE XIII. *Fitting the surface magnetisation m_1 at $\bar{\beta}_1 = 0.54914$.*

Ansatz	$L_{0,min}$	x	L_s	d	χ^2/DOF
47	8	-0.35303(7)	0.908(3)		31.87/6
47	12	-0.35341(12)	0.938(8)		14.37/5
47	16	-0.35377(16)	0.975(14)		3.13/4
48	6	-0.35367(14)	0.988(14)	0.12(2)	10.46/6
48	8	-0.35396(21)	1.029(27)	0.19(5)	6.97/5

where g_{h_1} denotes the partial derivative of g with respect to $h_1[L_0/l_{h_1}]^{y_{h_1}}$.

We have fitted the magnetisation at the boundary with the ansaetze

$$m_1(L_0) = c(L_0 + L_s)^x \quad (47)$$

with the free parameters c , L_s and x and

$$m_1(L_0) = c(L_0 + L_s)^x \times (1 + d(L_0 + L_s)^{-2}) \quad , \quad (48)$$

where we have included corrections $\propto L_0^{-1}$ and $\propto L_0^{-2}$, respectively. Using the Taylor-expansion, we have evaluated m_1 at $\bar{\beta}_1 = 0.54914$ and in order to estimate the effect of the uncertainty of our estimate of $\bar{\beta}_{1,sp}$ also at $\bar{\beta}_1 = 0.54916$. Results of fits with the ansaetze (47,48) using the data for $\bar{\beta}_1 = 0.54914$ are given in table XIII.

Repeating the fit with the ansatz (47) and $L_{0,min} = 16$ for the data taken at $\bar{\beta}_1 = 0.54916$ we get $x = -0.35280(16)$, $L_s = 0.935(13)$ and $\chi^2/\text{DOF} = 2.98/4$. Fitting the data for $\bar{\beta}_1 = 0.54916$ with the ansatz (48) and $L_{0,min} = 8$ we get $x = -0.35288(18)$, $L_s = 0.965(22)$, $d = 0.12(3)$ and $\chi^2/\text{DOF} = 6.08/5$. We see that the error of the exponent x as well as that of L_s is dominated by the uncertainty of $\bar{\beta}_{1,sp}$. As our final estimate we quote $x = -0.3539(13)$ and hence

$$y_{h_1} = 1.6461(13) \quad (49)$$

which is fully consistent with but less precise than the estimate obtained above, eq. (39). For the effective shift in the thickness of the lattice we quote $L_s = 1.0(1)$. Note that L_s should be equal to the sum of the extrapolation lengths at the two surfaces. For + boundary conditions we find in ref. [24] the result $l_{ex} = 0.96(2)$ for the + boundary conditions. Hence $l_{ex,sp} \approx 0$ for the BC1 model. This is consistent with our observation above that for the BC1 model corrections $\propto L_0^{-1}$ have a small amplitude.

We also have performed fits with the ansaetze (47,48), where $\bar{\beta}_{1,sp}$ is a free parameter. To this end we have used the Taylor series of the surface magnetisation m_1 in $\bar{\beta}_1$ around the simulation point. Such fits suggest $\bar{\beta}_{1,sp} = 0.54916(4)$, where the error is larger than that of our final estimate (27). Correspondingly, also the estimate of y_{h_1} cannot be improved this way.

B. The universal scaling function of the magnetisation profile

The magnetisation profile at the critical point behaves as [1-3]

$$m(z) = c L_0^{-\beta/\nu} \psi(z/L_0) \quad (50)$$

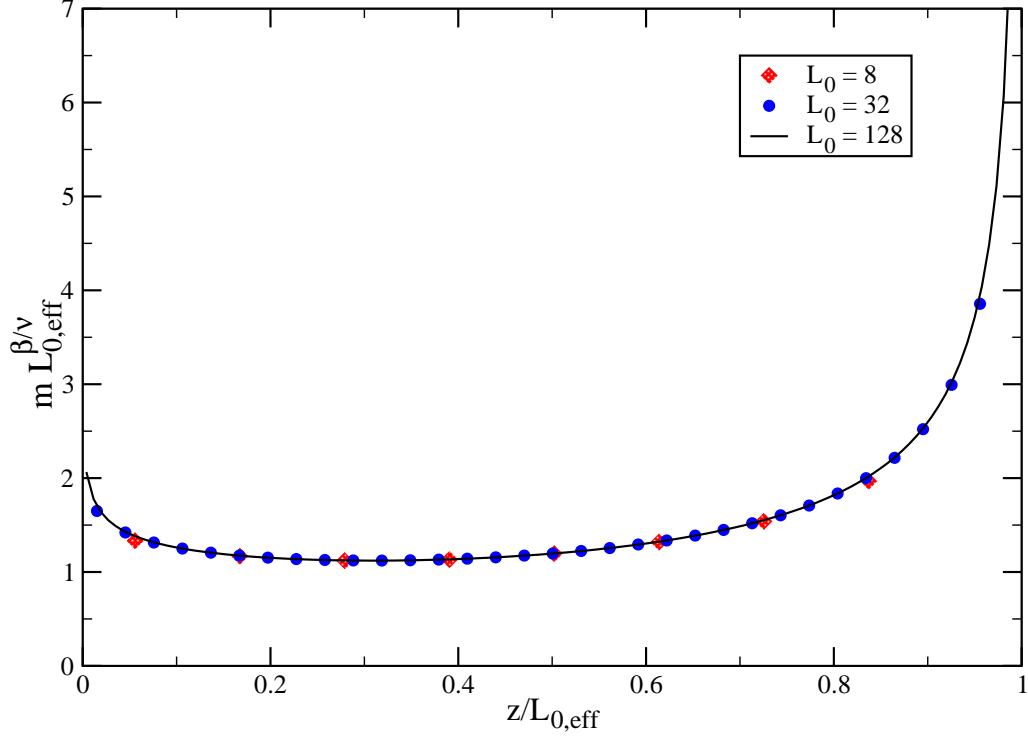


FIG. 2. We plot $m(z)L_{0,eff}^{\beta/\nu}$ as a function of $z/L_{0,eff}$, where z is the distance from the boundary with special boundary conditions. The data are taken at the bulk critical point. At the first boundary special boundary conditions and at the second + boundary conditions are applied. We give data for the thicknesses $L_0 = 8, 32$ and 128 . The line given for $L_0 = 128$ is obtained from a linear interpolation of the data points. We abstained from giving data for more thicknesses to keep the figure readable. Notice that the statistical errors are smaller than the symbols and the line shown. For a detailed discussion see the text. Colour online.

where z gives the distance from the boundary. The universal function ψ depends on the surface universality classes of the boundary conditions at the two surfaces of the film. In the neighborhood of the surface, the magnetisation follows a power law

$$m(z) = az^{-\beta/\nu + d - 1 - y_{h_1}} \quad . \quad (51)$$

Note that the exponent $-\beta/\nu + d - 1 - y_{h_1} = -0.1646(7)$ is negative and therefore the magnetisation is actually decreasing with increasing distance from the surface. This is in contrast to ordinary boundary conditions, where $y_{h_1} = 0.7249(6)$ [24], and therefore the magnetisation is increasing with the distance. Note that from scaling relations it follows that $\beta/\nu = (1 + \eta)/2$, where $\eta = 0.03627(10)$ for the three-dimensional Ising universality class [5].

Using the Taylor-expansion up to second order we have computed the magnetisation profile for $\bar{\beta}_1 = 0.54914$, which is our estimate of $\bar{\beta}_{1,sp}$. In figure 2 we have plotted $m(z)L_{0,eff}^{\beta/\nu}$ as a function of $z/L_{0,eff}$. In order to take corrections $\propto L_0^{-1}$ into account, we have replaced in eq. (50) the thickness L_0 by the effective one $L_{0,eff} = l_{ex,sp} + l_{ex,+}$. The distance from the boundary is given by $z = x_0 - 1/2 + l_{ex,sp}$. As discussed above, the extrapolation lengths take the values $l_{ex,+} = 0.96$ and $l_{ex,sp} = 0$. We see that the data for the three different thicknesses fall nicely on top of each other. The same holds for thicknesses not plotted here. Therefore

the curve obtained from $L_0 = 128$ should be a good approximation of the universal scaling function $\psi(z/L_0)$. We observe that, as discussed above, for small z the magnetisation is indeed decreasing with increasing z . At $z/L_0 \approx 0.31$ a very shallow minimum is reached.

VI. SUMMARY AND CONCLUSIONS

In this work we have studied the special point in the phase diagram of a semi-infinite system. We have accurately estimated the surface RG-exponents y_{t_1} and y_{h_1} that govern, along with the bulk RG-exponents y_t and y_h , the behavior of surface quantities at the special point. To this end, we have simulated the improved Blume-Capel model with two different surface interactions and the spin-1/2 Ising model on the simple cubic lattice. We have determined the surface RG-exponents from a finite size scaling analysis at the special point. In the presence of surfaces typically corrections $\propto L_0^{-1}$ appear, where L_0 is the linear extension of the finite system. Fitting data it is difficult to disentangle these from the leading bulk corrections $\propto L_0^{-\omega}$, where $\omega = 0.832(6)$ [5]. Therefore it is helpful that in the improved Blume-Capel model the amplitude of the leading correction to scaling vanishes.

In table XIV we compare our results with those obtained in previous Monte Carlo (MC) studies and computed by field theoretic methods. In previous MC studies only the spin-1/2 Ising model on the simple cubic lattice had been simulated. Only in ref. [21] results for the RG-exponents are quoted. However all authors give results for the exponents β_1 and most for Φ . In table XIV we have converted these estimates by using the scaling relations $\beta_1 = \nu(2 - y_{h_1})$ and $\Phi = \nu y_{t_1}$, where we have used $\nu = 0.63002$. In the case of y_{h_1} we observe that the estimates of refs. [21, 25] deviate by 9 and 6.6 times the combined error from our result. Notice that such deviations can be caused by corrections that are not taken into account in the ansatz. For a general discussion of this problem see section IIC. The fits performed in ref. [21] are in particular prone to this problem, since in the ansatz corrections $\propto L_0^{-3}$ are included while e.g. corrections $\propto L_0^{-2\omega}$ are missing. In the present work, we tried to estimate such systematical errors by comparing the results obtained by fitting with ansätze of a varying number of correction terms. In the case of y_{t_1} we see a quite good agreement with the results of refs. [20, 21]. In contrast, the estimates of refs. [18, 19, 27] are clearly larger than ours.

The surface critical exponents for the special point have been computed up to second order in the ϵ -expansion. Direct results have been obtained for the exponents $\eta_{||}$ [28] and Φ [29]. Starting from these two exponents and the bulk exponents, the remaining ones can be computed by using scaling relations. Naively inserting $\epsilon = 1$ one gets $\eta_{||} = -0.30$ and $\Phi = 0.68$ for three dimensions; see table VI of ref. [2]. In table XIV we give $y_{h_1} = (d - \eta_{||})/2$ and $y_{t_1} = \Phi/\nu$, where we have used $\nu = 0.63002$. The result for y_{h_1} is in quite good agreement with those from Monte Carlo simulations. In contrast, the estimate for y_{t_1} is by far too large. The authors of ref. [30] have pointed out that by resummation of the series, e.g. by Padé approximants this discrepancy can be resolved. The authors of ref. [30] have computed the surface exponents in a two-loop calculation in three-dimensions fixed. The numerical estimates quoted by the authors are obtained by using Padé approximants. The numbers given in table XIV are again obtained by using $y_{h_1} = (d - \eta_{||})/2$ and $y_{t_1} = \Phi/\nu$, where $\nu = 0.63002$. The results for y_{h_1} and in particular for y_{t_1} deviate clearly from those obtained from Monte Carlo simulations.

In addition to the estimates of the RG-exponents, our finite size analysis provides us with accurate estimates of the surface coupling $\bar{\beta}_{1,sp}$ at the special point for the three models that

TABLE XIV. Results for the surface RG-exponents of the special phase transition in the three-dimensional Ising bulk universality class.

Ref.	year	Method	y_{h_1}	y_{t_1}
[18]	1984	MC	1.72(4)	0.89(6)
[19]	1990	MC	1.71(3)	0.94(6)
[27]	1992	MC	1.65	1.17
[20]	1992	MC	1.624(8)	0.732(24)
[25]	1995	MC	1.623(2)	
[26]	1998	MC	1.635(16)	
[21]	2005	MC	1.636(1)	0.715(1)
this work	2011	MC	1.6465(6)	0.718(2)
[2, 28, 29]	1981	ϵ -exp, naive	1.65	1.08
[29, 30]	1998	ϵ -exp, resummed		0.752
[30]	1994	3D-exp, resummed	1.583	0.856

we have simulated. These estimates can be used in future studies of thin films. In particular, we intend to study the thermodynamic Casimir force in thin films in the neighborhood of the special point.

Furthermore we have studied the behavior of the surface transition in the neighborhood of the special point. Our numerical results follow the theoretical expectations. However the special point cannot be located accurately with such an approach.

Finally we have simulated a film with symmetry breaking boundary conditions at one surface and special boundary conditions at the other. The behavior of the magnetisation at the surface with special boundary conditions follows a power law. Its exponent can be expressed in terms of the RG-exponent y_{h_1} . The analysis of the data fully confirms our estimate of y_{h_1} given in table XIV. The magnetisation profile follows a universal function. This theoretical expectation is fully confirmed by the nice collapse of data that we observe for a large range of thicknesses L_0 of the film. An interesting feature of the magnetisation profile is that at the surface with special boundary conditions, which do not break the symmetry, the magnetisation is decreasing with increasing distance from the surface.

VII. ACKNOWLEDGEMENTS

This work was supported by the DFG under the grant No HA 3150/2-2.

-
- [1] K. Binder, “Critical Behaviour at Surfaces” in *Phase Transitions and Critical Phenomena*, Vol. 8, eds. C. Domb and J. L. Lebowitz, (Academic Press, 1983)
- [2] H. W. Diehl, Field-theoretical Approach to Critical Behaviour at Surfaces in *Phase Transitions and Critical Phenomena*, edited by C. Domb and J.L. Lebowitz, Vol. 10 (Academic, London 1986) p. 76.

- [3] H. W. Diehl, *Int. J. Mod. Phys. B* **11**, 3503 (1997) [arXiv:cond-mat/9610143]
- [4] M. N. Barber, “Finite-size Scaling” in *Phase Transitions and Critical Phenomena, Vol. 8*, eds. C. Domb and J. L. Lebowitz, (Academic Press, 1983)
- [5] M. Hasenbusch, *Phys. Rev. B* **82**, 174433 (2010) [arXiv:1004.4486]
- [6] Y. Deng and H. W. J. Blöte, *Phys. Rev. E* **70**, 046111 (2004).
- [7] Y. Deng and H. W. J. Blöte, *Phys. Rev. E* **68**, 036125 (2003)
- [8] C. J. Silva, A. A. Caparica, and J. A. Plascak, *Phys. Rev. E* **73**, 036702 (2006).
- [9] M. Hasenbusch, *Physica A* **197**, 423 (1993).
- [10] M. Campostrini, M. Hasenbusch, A. Pelissetto, and E. Vicari, *Phys. Rev. B* **74**, 144506 (2006) [arXiv:cond-mat/0605083]
- [11] R. Guida, J. Zinn-Justin, *J. Phys. A* **31**, 8103 (1998)
- [12] K. E. Newman and E. K. Riedel, *Phys. Rev. B* **30**, 6615 (1984)
- [13] M. Campostrini, A. Pelissetto, P. Rossi, and E. Vicari, *Phys. Rev. E* **60**, 3526 (1999)
- [14] F. J. Wegner *J. Math. Phys.* **10**, 2259 (1971)
- [15] U. Wolff, *Phys. Rev. Lett.* **62**, 361 (1989).
- [16] M. Hasenbusch, K. Pinn and S. Vinti, *Phys. Rev. B* **59**, 11471 (1999)
- [17] M. Saito and M. Matsumoto, “SIMD-oriented Fast Mersenne Twister: a 128-bit Pseudorandom Number Generator”, in *Monte Carlo and Quasi-Monte Carlo Methods 2006*, edited by A. Keller, S. Heinrich, H. Niederreiter, (Springer, 2008); M. Saito, Masters thesis, Math. Dept., Graduate School of science, Hiroshima University, 2007. The source code of the program is provided at “<http://www.math.sci.hiroshima-u.ac.jp/~m-mat/MT/SFMT/index.html>”
- [18] K. Binder and D. P. Landau, *Phys. Rev. Lett.* **52**, 318 (1984)
- [19] D. P. Landau and K. Binder, *Phys. Rev. B* **41**, 4633 (1990)
- [20] C. Ruge, S. Dunkelmann and F. Wagner, *Phys. Rev. Lett.* **69** (1992) 2465 C. Ruge, S. Dunkelmann, F. Wagner, and J. Wulf, *J. Stat. Phys.* **73**, 293 (1993).
- [21] Y. Deng, H. W. J. Blöte, and M. P. Nightingale, *Phys. Rev. E* **72**, 016128 (2005) [arXiv:cond-mat/0504173].
- [22] M. Caselle and M. Hasenbusch, *Nucl. Phys. B* **470**, 435 (1996) [arXiv:hep-lat/9511015]
- [23] M. Caselle, M. Hasenbusch, A. Pelissetto, and E. Vicari, *J. Phys. A* **35**, 4861 (2002) [arXiv:cond-mat/0106372]
- [24] M. Hasenbusch, *Phys. Rev. B* **83**, 134425 (2011) [arXiv:1012.4986]
- [25] C. Ruge and F. Wagner, *Phys. Rev. B* **52**, 4209 (1995)
- [26] M. Pleimling and W. Selke, *Eur. Phys. J. B* **1**, 385 (1998)
- [27] M. Vendruscolo, M. Rovere, and A. Fasolino, *Europhys. Lett.* **20**, 547 (1992)
- [28] J. S. Reeve, *Phys. Lett. A* **81**, 237 (1981)
- [29] H. W. Diehl and S. Dietrich, *Phys. Rev. B* **24**, 2878 (1981); H. W. Diehl and S. Dietrich, *Z. Phys. B* **50**, 117 (1983)
- [30] H. W. Diehl and M. Shpot, *Phys. Rev. Lett.* **73**, 3431 (1994); H. W. Diehl and M. Shpot, *Nucl. Phys. B* **528**, 595 (1998)